

Article

# Contribution to the Mineral Chemistry of the Proterozoic Aravalli Mafic Meta-Volcanic Rocks from Rajasthan, NW India

Janina Wiszniewska <sup>1,\*</sup>, Anna Grabarczyk <sup>2</sup>, Ewa Krzemińska <sup>3</sup> and Talat Ahmad <sup>4</sup>

<sup>1</sup> Environmental Geology Department, Polish Geological Institute-National Research Institute, Rakowiecka 4 Str., 00-975 Warsaw, Poland

<sup>2</sup> Institute of Geochemistry, Mineralogy and Petrology, Faculty of Geology, University of Warsaw, Żwirki i Wigury 93 Str., 02-089 Warsaw, Poland; anna.grabarczyk@uw.edu.pl

<sup>3</sup> Micro-area Analysis Laboratory, Polish Geological Institute-National Research Institute, Rakowiecka 4 Str., 00-975 Warsaw, Poland; ekrz@pgi.gov.pl

<sup>4</sup> Department of Geology, University of Delhi, 110067 Delhi, India; tahmad001@gmail.com

\* Correspondence: janina.wiszniewska@pgi.gov.pl; Tel.: +48-609849355

Received: 10 June 2020; Accepted: 16 July 2020; Published: 18 July 2020



**Abstract:** Field, petrological and mineral chemistry for meta-volcanic rocks from the Aravalli sequence (Aravalli Craton, India) are presented. Field evidence such as volcanic flows and suspect pillow lava structures, dominant Fe-tholeiite lava flows intercalated with quartzites and argillaceous sediments, indicate rift tectonic environment. Primary mineralogy was obliterated during post-magmatic processes such as metamorphism corresponding to the greenschist to lower amphibolite facies conditions. The rock's mineral composition was overprinted by plagioclase–chlorite–amphibole–epidote assemblage. The relicts of clinopyroxene were observed. The P–T estimation indicates a temperature of 550–600 °C for the pressure ranging from 3.0 to 7.0 kbar for the majority of amphiboles and 8.0–10.7 kbar for the minority. Geochemically, these rocks are komatiitic (picritic) and high-Fe tholeiitic basalts with 45.06–59.2 wt.% SiO<sub>2</sub> and MgO content from 5 to 22.4 wt.% and Mg# of 17 to 71. They show large-ion lithophile elements (LILE) and light rare-earth elements (LREE) enrichment. Chondrite normalized rare-earth elements (REE) patterns for the Aravalli lava are moderately enriched with (La/Sm)<sub>N</sub> = 1.1–3.85, (La/Yb)<sub>N</sub> from 1.49 (komatiites) to 14.91 (komatiitic basalts). The trace element systematics with the negative Nb, P and Zr anomalies reflect their derivation from enriched sub-continental lithospheric sources, although minor crustal contamination cannot be ruled out. Aravalli rocks are considered to represent the transition from continental rift magmatism to shallow submarine eruption.

**Keywords:** pillow lava; Fe-tholeiite; basaltic komatiite; Aravalli craton

## 1. Introduction

The granite–greenstone belts, preserved in ancient cratonic nuclei of continents, provide significant geological evidence for the evolution of the Earth in its early stages [1–3]. Archean greenstone belts are predominantly composed of variably metamorphosed and deformed ultramafic-mafic to felsic volcanic and silici-clastic sedimentary rocks [4,5].

Volcanogenic and volcano-sedimentary rocks of the Archean to Proterozoic greenstone belts are best known from South Africa (Barberton Greenstone Belt), Australia (Pilbara Craton), and western Greenland (Iska Greenstone Belt) but also from the Indian sub-continent, where a few greenstone complexes were recognized including an Aravalli craton with an Aravalli-Delhi Fold Belt in northwestern part of India.

The Aravalli Mountain Range of Rajasthan is an 800-km long mountain belt, with a long geological history from the Archean to Neoproterozoic period [6]. The presence of two generations of greenstone belts was identified [7]. The polycyclic Proterozoic orogenic processes, involving crustal thickening and thermal perturbations, successively obscured many of their original mineralogical features, thus all relics of the original structures are particularly valuable objects for these genetic investigations.

The occurrence of metamorphosed komatiitic (picritic) with suspect pillow lava and lava flows in association with Fe-tholeiites, quartzites, basal conglomerate, calcareous and argillaceous meta-sediments are recorded from the Aravalli mafic-ultramafic magmatic sequence [8], and are similar to the Archean Bundelkhand craton in Central India [9]. The remnants of basalt volcanism preserved as suspect pillow and lava flow structures were discovered in natural outcrops between the Nathdwara and Delwara towns, north of Udaipur city. These rocks document the proximity to the ancient eruption center and textural features formed during rapid solidifying processes.

This contribution presents new comprehensive mineral chemical data along with the earlier results for our geochemical investigations based on whole rock major and trace element composition, in order to characterize alteration processes and to understand the metamorphic conditions, petrogenesis and evolution of the mafic lavas. Particular emphasis is placed on the determination of the mineral composition of metamorphic assemblage, which has not yet been accurately performed on the Aravalli rocks. The studied meta-basalt samples were collected from near the Kajiwara and Matata villages, south of Nathdwara town, shown as a star in Figure 1. The meta-volcanic rocks are intercalated with conglomerate, grit and arkosic horizons at the base, followed by quartzitic and phyllitic units. The conglomerates contain clasts derived from the Banded Gneissic Complex (BGC) basement, the grit and arkoses also have more derivatives of granitic rocks from the BGC, probably indicating lesser transportation and quick deposition of these meta-sediments. This is followed by the deposition of a more mature quartzitic horizon, indicating longer transportation to lose the feldspars and concentration of clean-washed quartz grains. This horizon is followed by the phyllitic sequence, probably indicating a deepening of the basin. All through the described sedimentary sequence, meta-basalts are observed as intercalated with these sediments, probably indicating a rift tectonic environment for the eruption of the studied basalt [8,10].

## 2. Materials and Methods

The existence of the 3.7–3.5 Ga old Aravalli proto-continent is present in the Aravalli region (Northwest India), confirmed by detrital zircons in the sediments [11–14]. The initial stage of the continental growth took place in Paleoproterozoic and continued during the Proterozoic period. This long-lasting process of cratonization resulted due to the generation of poly-phase granite–gneiss terrains, represented by the Banded Gneissic Complex (BGC) [15]. It is believed that the BGC became stabilized at ~2.5 Ga and then was overlain by two Proterozoic supra-crustal complexes: The Aravalli and Delhi Super-groups, formed in 2.3–1.4 Ga in extensional regimes. These two Aravalli and Delhi orogenic belts evolved one after the other, separately in space and time, comprising together the Aravalli Mountain Range. Geochronological data indicate ca. 1.72–1.0 Ga ages for the polyphase deformation and metamorphism related to the collision and the subsequent orogenesis [7]. The relationship between the BGC basement rocks and the cover is contentious, similarly as in many strongly deformed Proterozoic fold belts. The typical granite–greenstone belt sequences of the Aravalli Super-group are associated with gneisses of the BGC basement.

The Aravalli Mountain Range have been assigned to three litho-stratigraphical units, which correspond to three independent geological cycles [10,15–17]: (1) crystalline basement of Rajasthan, known as the Banded Gneissic Complex (BGC), (2) Aravalli Super-group, and (3) the youngest Meso-Neoproterozoic Delhi Super-group (Figure 1).

The Aravalli Super-group has an unconformable relationship with BGC all along the entire margin of the Aravalli fold belt. The Aravalli Super-group has been additionally subdivided into three lithological Formations: The Delwara Fm., Jhamarkotra Fm. and Zawar Fm. The lowest Delwara

Formation north of Udaipur comprises a thick sequence of mafic and ultra-mafic (komatiitic) volcanic rocks [8,11], generally referred to as the Delwara–Nathdwara volcanic sequence [7]. Based on the available radiogenic data of komatiite and tholeiite of 2.3 Ga was determined as the initial age of rifting of the BGC basement and eruption of the basal Aravalli volcanic sequence [16,18]. Collectively, geochronological data, based on Nd isotopic values, suggest that komatiitic and tholeiitic rocks erupted between 2.3–1.8 Ga from enriched and heterogeneous mantle source regions as part of the sub-continental lithospheric mantle of the Aravalli Craton [7,16]. The rocks of the Aravalli super-group have undergone later greenschist (in the southern part) to upper-amphibolite grade metamorphism in the northern part [17] and have undergone three main phases of folding [19].

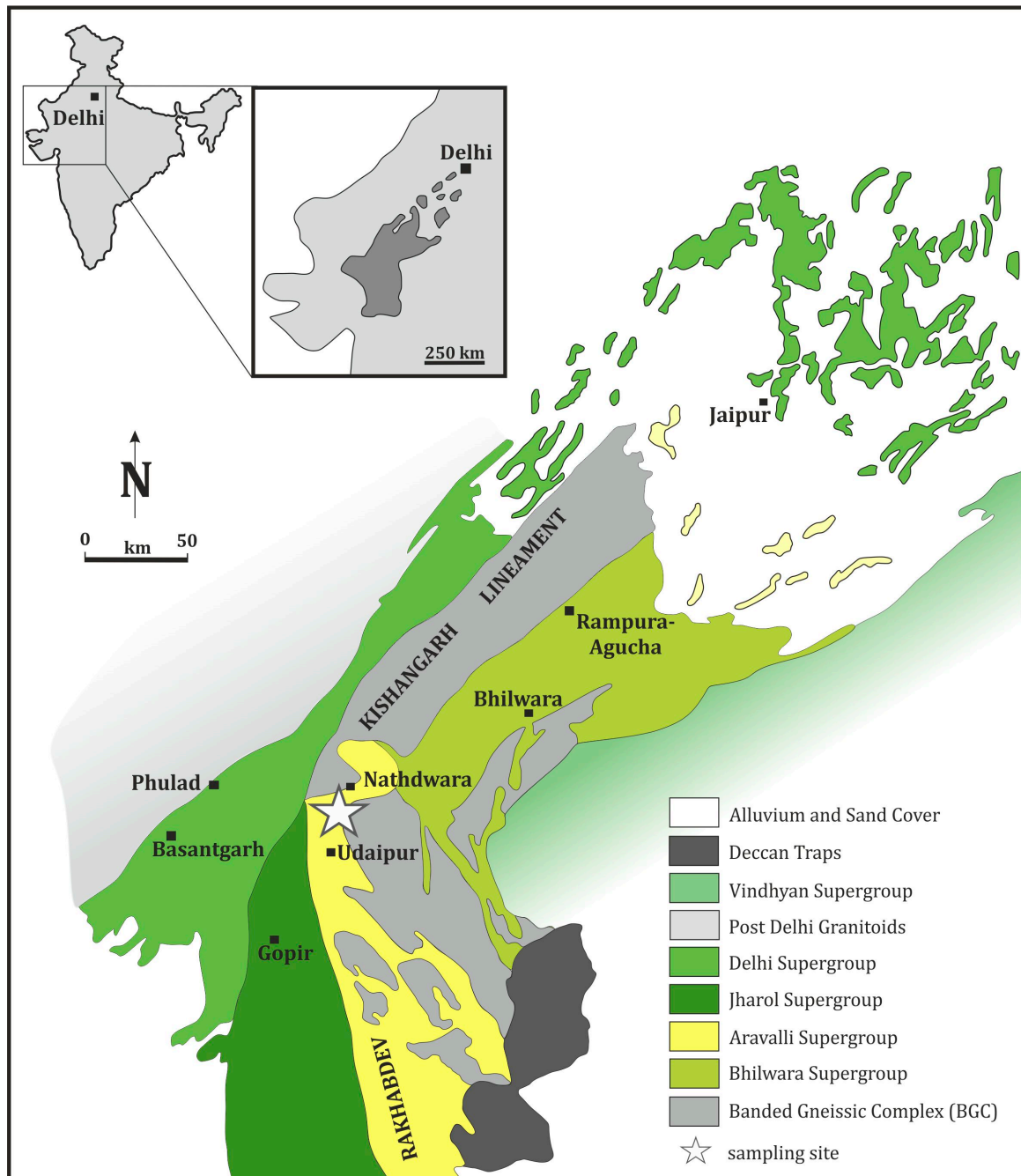


Figure 1. Simplified regional geological map of the Aravalli–Delhi orogeny after [20].

The studied samples come from the same structural unit—The Aravalli Super-group. Electron microprobe analysis (EPMA) of mineral chemistry was undertaken using a CAMECA SX 100 (equipped with wavelength dispersive spectrometry) instrument in the Electron Microprobe Laboratory of the Inter-Institute Analytical Complex for Minerals and Synthetic Substances in the University of Warsaw and the Polish Geological Institute. Analyses on polished thin sections were performed with 15 kV accelerating voltage and a beam current of 10 nA. Collected natural and synthetic silicates and oxides were used for calibration. Raw data were corrected by the ZAF method which includes corrections for atomic number effects (Z), absorption (A) and fluorescence (F).

The whole-rock samples were analyzed for major elements and some trace elements in the Polish Geological Institute-National Research Institute (PIG-NRI) laboratory. Major elements and trace element analyses for Ba, Co, Cr, Cu, Ni, Rb, Sr, V, Y, Zn, and Zr were analyzed by the X-ray fluorescence (XRF) technique but REE and the selected trace elements Nb, Hf, Ta, W, Tl, Bi, Ga, Ge, Sn, Sb, Cs, Th and U were analyzed using inductively-coupled plasma-mass spectrometry (ICP-MS) at the Polish Geological Institute, Warsaw.

### 3. Results

#### 3.1. Field Occurrence

Meta-volcanic rocks from the basal Aravalli sequence in Rajasthan are best exposed between Nathdwara and Delwara, north of Udaipur city (Figure 1). The supra-crustal rocks of Aravalli sequence have undergone greenschist to lower-amphibolite facies metamorphism and polyphase deformation. These relatively high magnesium rocks occur at the contact of the basal Aravalli sequence with BGC (Figure 1). At some places, however, the amphibolites derived from meta-basalts have preserved relict pillow lava structures (Figure 2a,b). This is the first report of suspect pillow lava structures within the basal volcanic rocks of the Aravalli super-group with a spinifex-like texture, now occurring as fibrous amphiboles, observed on the surface of the pillows pile (Figure 2c,d). The suspect pillow lava outcrops were found on the top of the Nathdwara hills around Kajiawas village. They are formed in a separated 1.0–1.5-m high to 0.5–0.8-m wide band of a hard black pile of pillow-like lava sequence. This pillow-covered crust, about 2.0–5.0 cm thick, is enriched in platy, fibrous or acicular-like post-pyroxene amphibole crystals, around 0.5–2.0 cm long and 0.1–0.2 cm wide in a glassy matrix. The internal part of the pillows is coarser grained, composed of dark green to dark grey and black minerals of amphibolite composition.

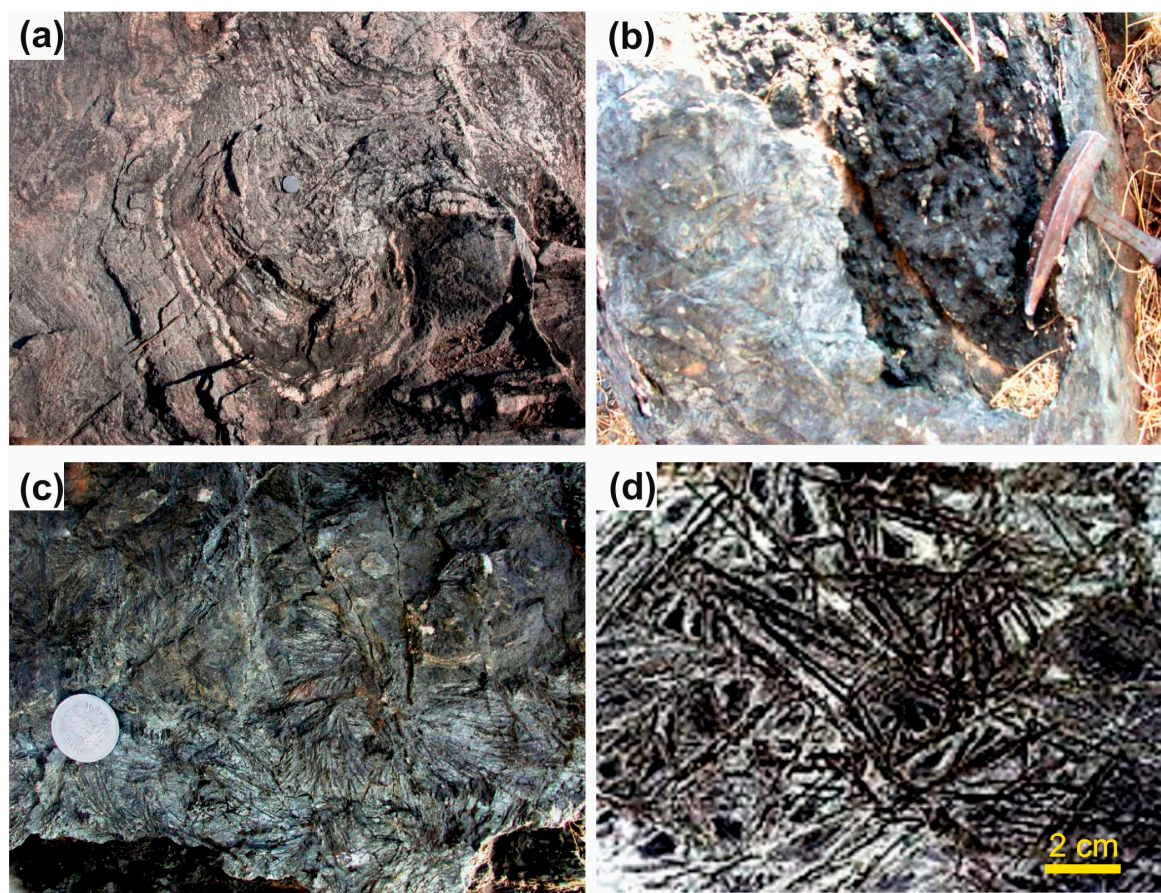


**Figure 2.** Field photographs showing morphology of the pillow lava outcrops at the Aravalli area. (a) pillow structures showing deformation, (b) oval shape of the pillow lava in the Aravalli area with visible spinifex-like texture on the surface, (c,d) fibrous and platy amphibole on the Aravalli pillow lava surface. Note the hammer and the coin for scale.

### 3.2. Mineral Chemistry of the Suspect Pillow Lava

The greenschist to amphibolite facies metamorphism and secondary alteration obliterated the primary mineralogy. These meta-basalts are characterized by mineral assemblage including: amphibole  $\pm$  plagioclase  $\pm$  chlorite  $\pm$  epidote  $\pm$  ilmenite  $\pm$  hematite  $\pm$  sulphides. The amphibolites range from coarse- to medium-grained, with a pillow-like lava surface.

The suspect pillow lava from Aravalli has a preserved, fibrous, spinifex-like texture (Figure 2c,d). Such type of crystal arrangement develops as a result of large thermal gradients, coupled with conductive and radiative heat transfer within olivine or/and pyroxene crystals fixed in the cool upper layers of the lava flows [21,22]. All samples collected from natural outcrops are found to consist of amphibolite facies mineral assemblage, dominantly comprising crystals of calcic amphibole (Figure 3a–d) with only single pyroxene relicts accompanied with plagioclase (Figure 4a,b), apatite, ilmenite, chlorite (Figure 3d or Figure 4a) and epidote (Figure 4c,d) with allanite (Figure 4c). Small baddeleyite grains were also observed.

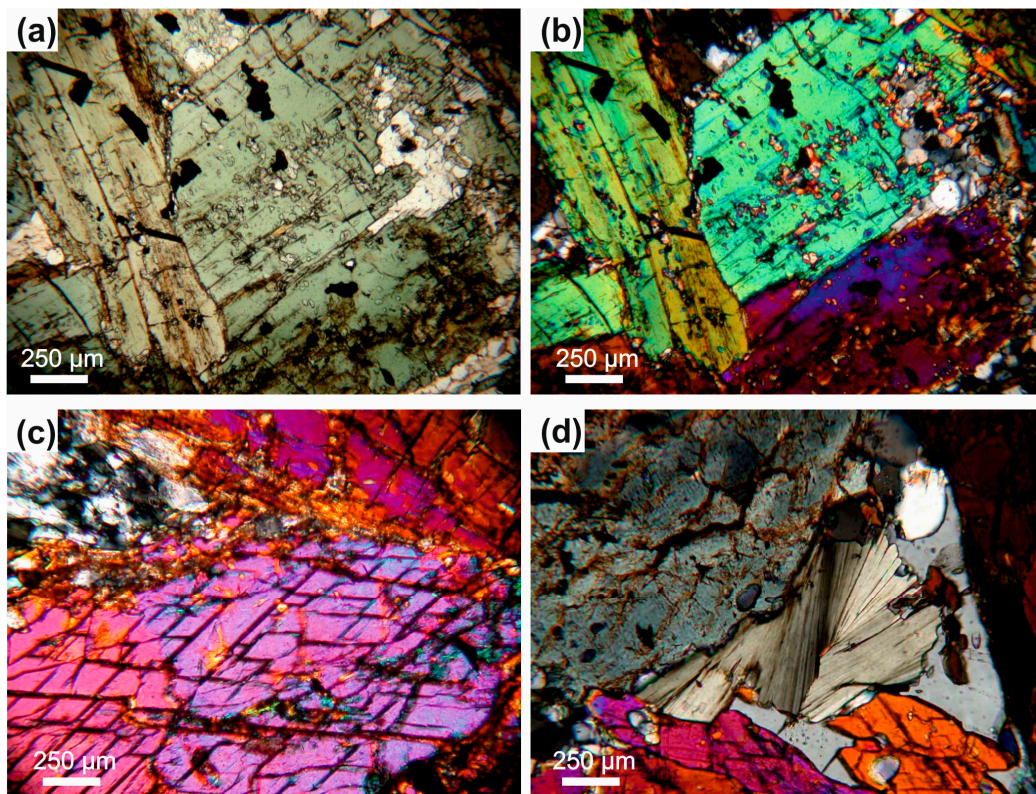


**Figure 3.** Photomicrographs of the studied samples from the Aravalli area. (a–c) pseudomorphic large Ca-amphibole grains making spinifex-like texture in Aravalli pillow lava, (d) retrogressive Mg chlorite after amphibole.

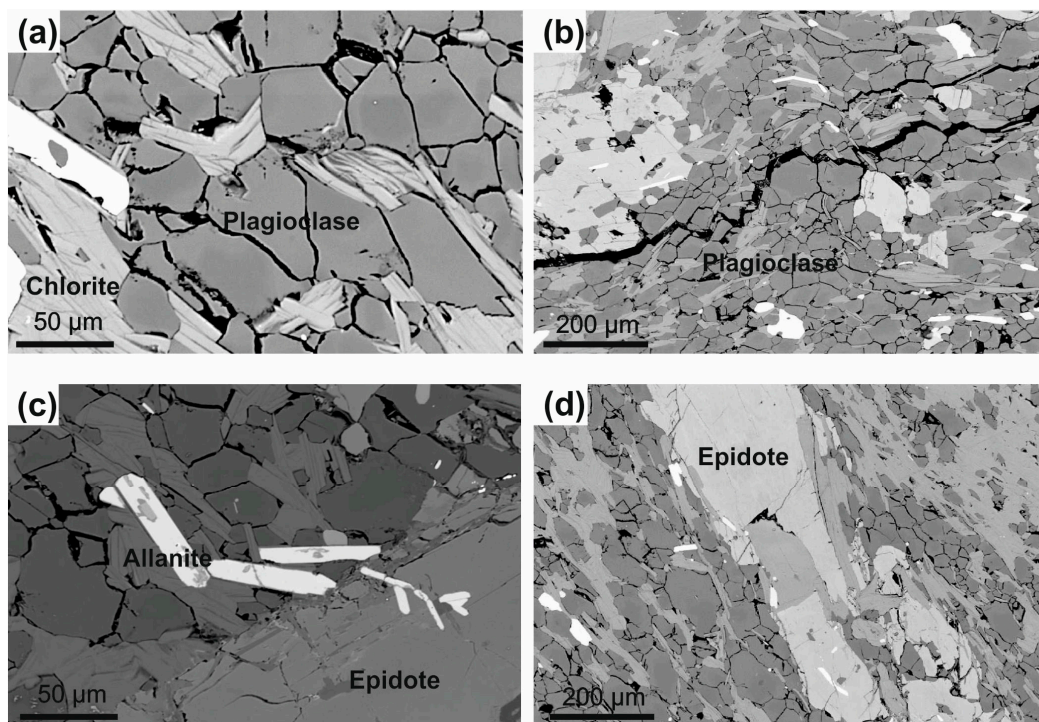


**Figure 4.** Backscattered-Electron (BSE) micrographs of the studied samples from the Aravalli area. (a) retrogressive Mg chlorite with plagioclase grains, (b) euhedral plagioclase grains, (c,d) accessory allanite and epidote after plagioclase.

### 3.2.1. Amphibole

Euhedral, elongated Ca-amphiboles with visible zonation, which resulted in variable content of Fe and Mg, but also  $\text{SiO}_2$ , are dominant minerals from the pillow-like lava basalts. The slender amphibole crystals have a radial orientation to random and intersecting arrangement, giving rise to spherulitic-type/or spinifex-type textures. The rocks contain predominantly large euhedral green-colored amphibole grains (Figure 3a–c) with randomly oriented ilmenite intergrowths, spinel and apatite within amphibole crystals. An amphibole composition from the collected Aravalli pillow lava samples was projected onto an amphibole classification diagram according to the nomenclature of [23] (Figure 5; Table S1). The EPMA data indicate that amphibole compositions are straddled between magnesio-hornblende and pargasite with a pronounced fluctuation of alkali content visible in the  $A^*$  value. A core–rim relationship was observed in some places. A wide range of Mg# (defined as  $\text{Mg}/(\text{Mg} + \text{Fe}^{2+})$ ) from 0.40 to 0.82 is observed, where the samples from the inner part of the pillow-like lava (AR-6C and AR-6E) are less magnesian than that of the outer zones (AR-6A and AR-6A(2)). The Si content ranges from 6.11 to 7.23 apfu. The content of titanium is always low, in the range of 0.17 to 0.44 wt.% of  $\text{TiO}_2$  with a single-grain content above 1 wt.%. The analytical data show a variable  $\text{Al}_2\text{O}_3$  content, ranging from 7.2 to 17.1 wt.%. These variable alumina and Ti contents are not related to the pillow lava zone.

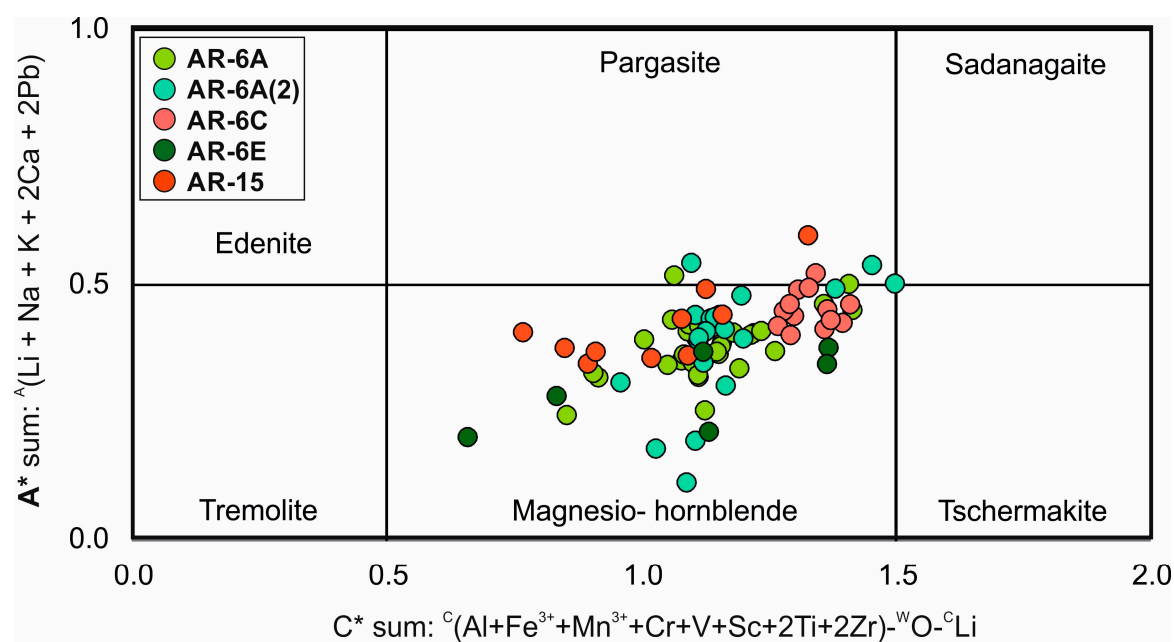


**Figure 5.** Ca-amphiboles chemistry from the ortoamphibolites from the Aravalli. Plot of the EMPA data in the calcic amphibole classification diagram [23].  $A^* = \text{Li} + \text{Na} + \text{K} + 2\text{Ca} + 2\text{Pb}$ ;  $C^* = \text{Al} + \text{Fe}^{3+} + \text{Mn}^{3+} + \text{Cr} + \text{V} + \text{Sc} + 2\text{Ti} + 2\text{Zr} - \text{W} - \text{O} - \text{Li}$ .

### 3.2.2. Pyroxene

The only fragments of primary pyroxene grains were preserved within larger amphibole crystals. All pyroxene grains were substituted by amphibole during the metamorphism of the pillow lava. They were observed in microprobe, thus only eight points of this relict group were analyzed (Table S2). Pyroxenes from two samples analyzed have an igneous origin, varying from augite (dominant) to pigeonite and clinoenstatite, classified after [24] (Figure 6a). The augite relicts with a relatively small array of Ca (0.486–0.509 apfu; Table S2) have Mg# ranges from 0.55 to 0.74. The Cr content is below detection limit, but they have some amount of Na (0.11 to 0.48 wt.%  $\text{Na}_2\text{O}$ ), reflecting aegirine molecules, as detected for alkali basalts.

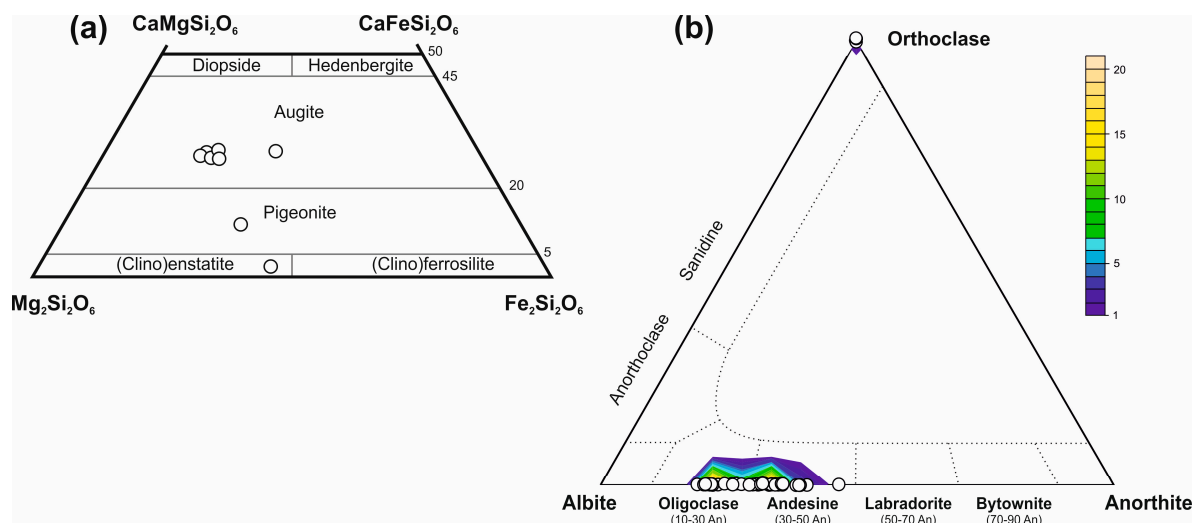


**Figure 6.** (a) pyroxene chemistry of the orthoamphibolites from the Aravalli area, plot of the EPMA data in the pyroxene classification diagram after [20], (b) plagioclase chemistry of the orthoamphibolites from the Aravalli area, plot of the EMPA data in the feldspar classification diagram.

### 3.2.3. Feldspar

These minerals, found as plagioclase and K-feldspar, were observed through the 47-point analysis (Figure 6b; Table S3). Some of the currently recognized plagioclase remnants, due to the recrystallization to other minerals like epidote, are igneous, which is proven by their original euhedral tabular habit. There is also a dominant group of fine-grained feldspars, probably of metamorphic origin. Plagioclase represents a variable chemical composition with a mostly alkaline character and the visible metamorphic deformation. Microprobe analyses indicate almost equal amounts of andesine and oligoclase with two graphically pronounced maxima for An<sub>33</sub> and An<sub>20</sub> plagioclase composition (Figure 6b; Table S3). It is not possible to observe a clear core–rim relationship since most analyzed crystals are heterogeneous with a random composition or a homogeneous composition. The presence of a secondary potassium feldspar is also detected.

### 3.2.4. Chlorite

Chlorite is also common in some parts of pillow lava samples (Figure 3d or Figure 4a). This mineral phase results from thermal modifications and/or the replacement of primary Fe–Mg pyroxene or amphibole minerals. The analyses of a total of 25 points was conducted (Table S4). The EPMA data document a small dispersion (variation in the analysis of the composition of the same sample) with a uniform Fe# parameter  $Fe/[Mg + Fe] = 34\text{--}40$  mol%. This is considered to be a typical feature of Fe, Mg-chlorite with composition corresponding to that of ripidolite, based on [25]'s classification, used by [26] in an excel spreadsheet. No significant variation is found in the mineral core–rim relation, as the minerals were found to have a homogeneous composition. This metamorphic mineral originates in low metamorphic grades, restricted to greenschist facies.

### 3.2.5. Ilmenite

The TiO<sub>2</sub> content of the ilmenite from Aravalli pillow lava varies from 51.08 wt.% to 53.08 wt.%, which is close to the theoretical ilmenite 52.75 wt.% composition. The minor variations could be due to the leaching of other cations. The FeO content of the ilmenite varies from 43.56 wt.% to 46.57 wt.%. The large range of FeO in the ilmenite could be due to hematite exsolutions. The MnO content of ilmenite in different sections of the pillow varies from 2.25 wt.% to 3.97 wt.% or 1.45 wt.% to 2.03 wt.%, while the MgO content varies from 0.04 wt.% to 0.08 wt.%, with one higher content of 0.276 wt.%. (Table S5) The presence of significant amounts of manganese indicates that the Aravalli ilmenite constitutes a

solid solution series with pyrophanite and smaller amounts of geikelite. As a result of these solid solutions, the  $\text{TiO}_2$  content of ilmenite reveals some variation in comparison to an ideal value. The amounts of  $\text{V}_2\text{O}_5$ ,  $\text{Al}_2\text{O}_3$ ,  $\text{Cr}_2\text{O}_3$ ,  $\text{NiO}$ ,  $\text{ZnO}$  are not significant or below the detection limit. Whereas typical igneous ilmenite from mafic and ultramafic rocks has 0.5 wt.% to 10 wt.% of  $\text{MgO}$  and less than 1 wt.% of  $\text{MnO}$ , it is apparent that the ilmenite from Aravalli pillow lava represents igneous grains that have been compositionally modified by diffusion processes during metamorphism [27].

### 3.3. Geothermo-Barometers

The amphiboles, as a mineral phase stable over a wide range of pressure and temperature from 1 to 23 kbar and 400 to 1150 °C [28], are an effective tool used for the estimation of P-T conditions of various Ca-amphibole-bearing rocks. The P-T parameters are usually determined based on the composition of amphibole-plagioclase pairs or amphibole-liquid calibration or amphibole-only calculation. This last option, independent of magma composition, was tested in Aravalli samples. The lava pillows contain different forms of amphibole (Figures 3 and 4), accompanied or not accompanied with plagioclase of oligoclase to andesine composition, which suggests that these rocks did not achieve a state of equilibrium.

There are several successfully tested thermometers and barometers designed mostly for the igneous system. A few amphibole-only formulas allow us to approximate a range of pressure and temperature of metamorphic rocks. In these equations, the Ca-amphibole composition has to be calculated on the basis of 23 oxygen anhydrous mineral formula (Table S6).

The Ti thermometer of [29] applied to a magmatic system can be also used for sub-solidus hornblende. The temperatures, obtained according to their semi-empirical equation in most of the Aravalli analysis (Table S6), suggest a range of 600–550 °C (Figure 8a). These amphiboles were formed by the sub-solidus alteration of cumulus minerals, thus the Ti content was dependent on the availability of the Ti bearing phase (ilmenite). Consequently, the amphiboles may not contain the maximum amount of Ti and the thermometer may yield a minimum temperature [29].

The correlation between Al in hornblende and pressure was examined by the formula of [29–31] (Table S6).

An additional two formulas were also tested. Single-phase barometers, working with the total aluminum content of amphibole of [32] (Table S6), also provide two stages and falling in the ranges of pressure 3.0–7.0 (but mostly in the range of 5.0–6.0 kbar) and 8.0–10.7 kbar, mainly for the AR-6C sample, from the inner part of the pillow lava (Figure 8a). In contrast to the formula of [33], this showed a wider range of the pressure—4–14 kbar and 14–18 kbar. Some of them seem to be overstated, as they are too high (Table S6).

On the other hand, according to [34], amphiboles with Si of 7.3 (apfu) or less are generally considered magmatic and Si higher than 7.3 (apfu) is not a truly magmatic amphibole. In these terms, the Aravalli amphibole crystals plot as igneous, far off of the metamorphic field (Figure 7a). They display a variation of Si content and a sum of Na, Ca, K, whose particular values overlap with the population commonly found in magmatic arc amphiboles. The case of this (Na + Ca + K vs. Si) relationship should be explained, rather, as an indicator of meta-igneous origin. The amphibolite facies metamorphism recrystallized the probable reach of pyroxene protolith. An almost-analogous diagram (Na + K) vs. Si is used as a discriminator of protolith for ortho- vs. para-amphibolite [35].

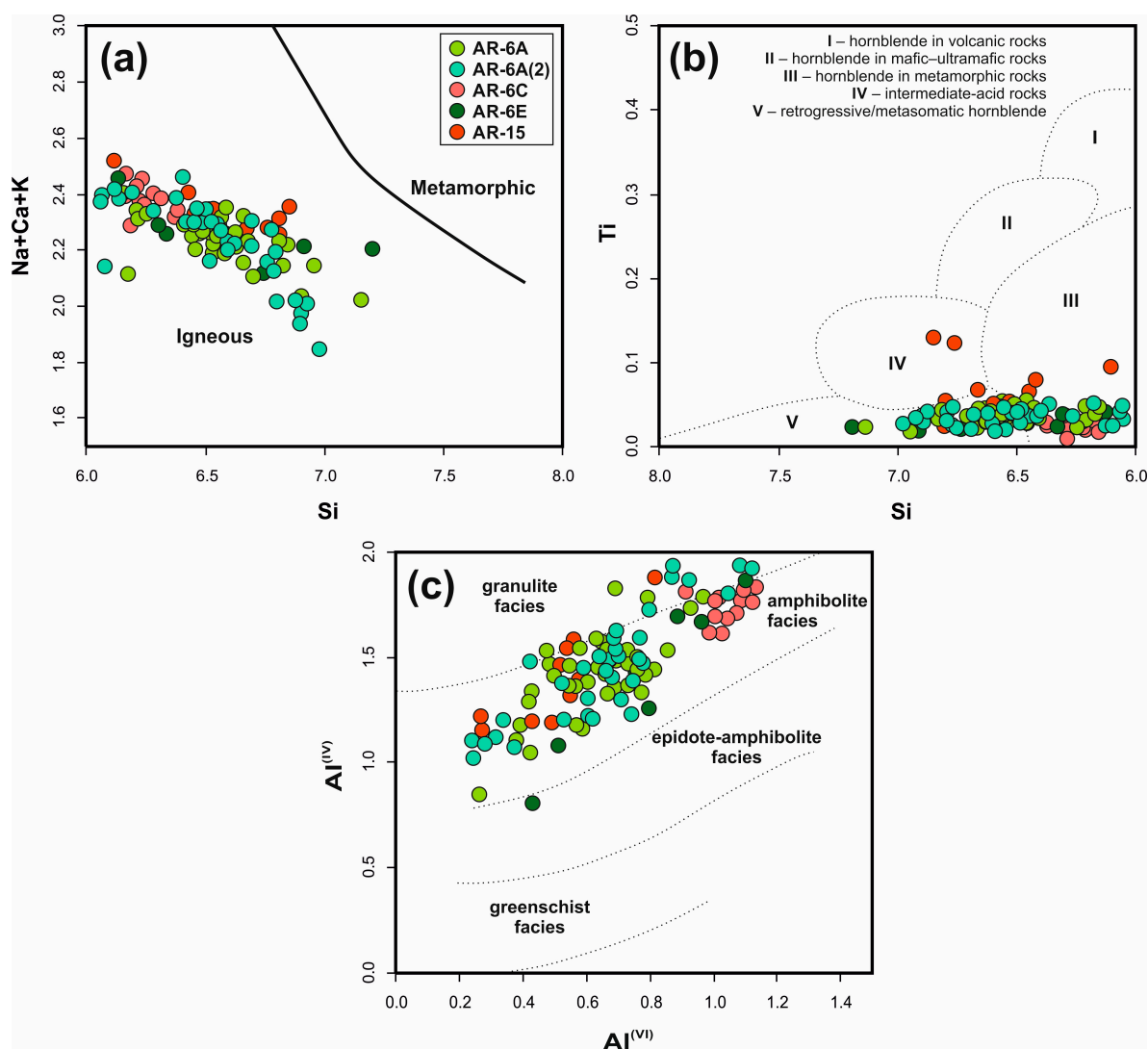


**Figure 7.** Discrimination diagrams for hornblendes from the Aravalli area orthoamphibolites. (a) Na + Ca + K vs. Si diagram, (b) Si vs. Ti diagram for hornblendes after [36], (c) Al<sup>VI</sup> vs. Al<sup>IV</sup> diagram after [37].

The condition of amphibole formation shows that they crystallized in a medium-temperature regime, typical for retrogressive changes. This is confirmed by the low Ti content in amphibole grains from pillow lava, which places them in the field of the metamorphic rocks or even amphiboles resulting from metasomatic processes (Figure 7b) [36].

More detailed conclusions can be drawn from the Al<sup>IV</sup> vs. Al<sup>VI</sup> diagram (Figure 7c) [37], where amphiboles from pillow-like lava are located within the field of amphibolite facies, but they can be divided into two groups: high Al amphiboles close to granulite facies borders and lower-Al amphiboles, clearly showing a retrogressive trend with decreasing temperature. Metasomatism is documented by the occurrences of the feldspathic and chloritic veins within the most-altered zones.

Complementarily, the chlorite-bearing altered parts of amphiboles were used for the chlorite thermometry, defining the last stage of metamorphic evolution. The studied chlorites based on crystal-chemical classifications have constant ripidolite compositions with (Fe/(Fe + Mg)), which range from 0.364 to 0.433 (Table S4). The Fe-chlorite crystallization temperatures were calculated on a basis of three different calibration methods by [38–40] that indicate similar temperature ranges from  $330 \pm 16$  °C to  $290 \pm 8$  °C (Figure 8b). These temperature ranges refer to greenschist facies metamorphism (typically 300–450 °C and 1–4 kbar pressures), and the most characteristic minerals in metabasalt remain as chlorite, actinolite composition amphibole, and Na rich plagioclase (albite) ± epidote.

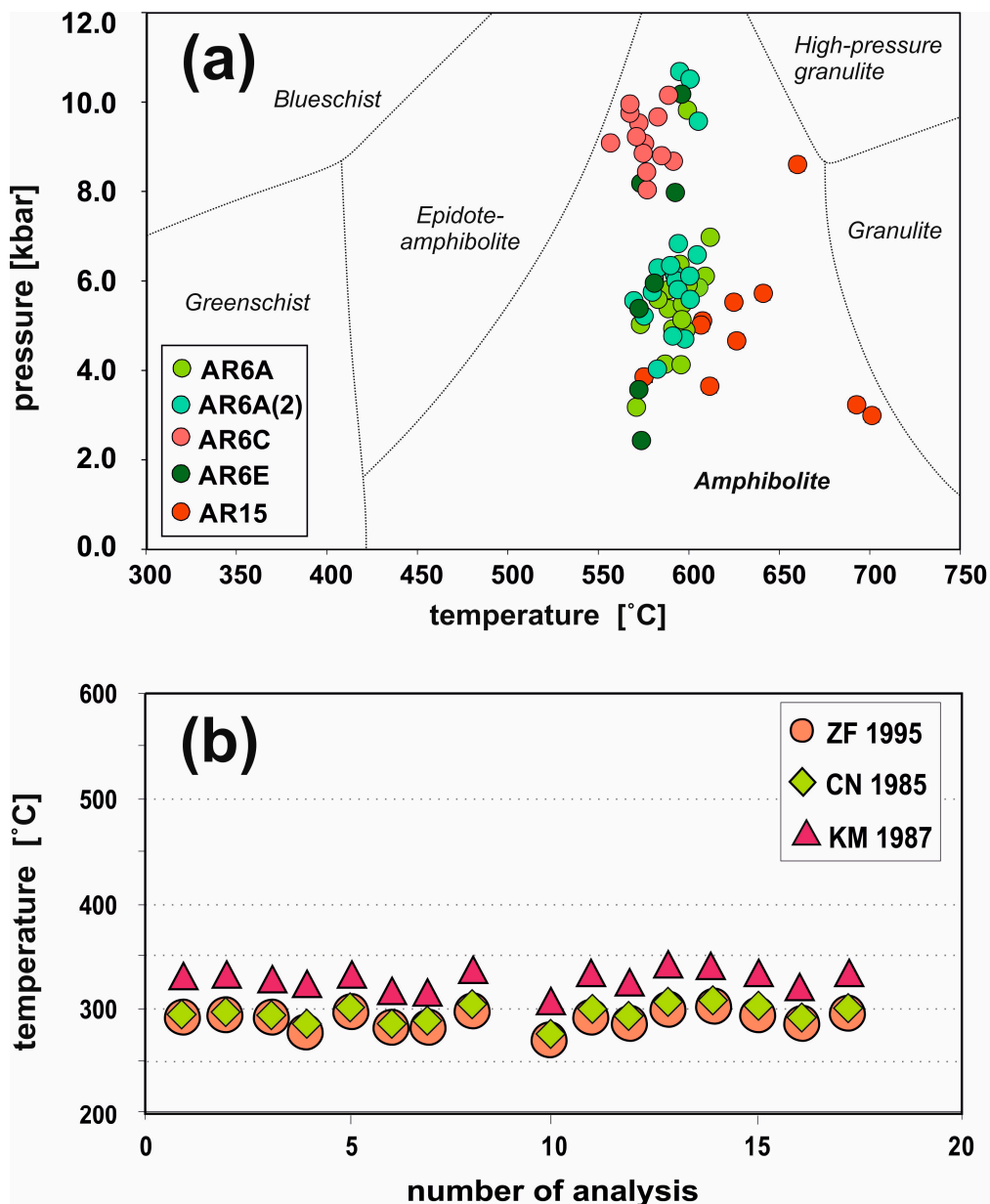


Figure 8. (a) P-T condition estimation after [29,32] (b) pressure and temperature conditions of metamorphic processes calculated on chlorite formation conditions after ZF [38], KM [39] and CN [40].

### 3.4. Geochemistry of Aravalli Pillow Lava

Some samples from the pillow-like lava surface have high loss on ignition (LOI), suggesting that hydrothermal alteration was significant and excludes the use of these samples for further considerations. This is confirmed by the presence of the secondary minerals, such as calcite, chlorite and epidote, which were identified in veinlets. The inner part of pillow lava represents one sample (AR-6C), whose composition is presented in Table 1.

**Table 1.** Major and trace element averages for AR-6C sample and tholeiites, komatiitic basalts and komatiites from Aravalli area.

Sample	AR-6C	Tholeiites (n = 10)		Komat. Basalts (n = 6)		Komatiites (n = 6)	
		Average	SD*	Average	SD*	Average	SD*
Oxides wt.%							
SiO <sub>2</sub>	45.06	52.96	3.57	53.62	1.26	52.15	1.96
TiO <sub>2</sub>	1.26	1.46	0.62	1.13	0.28	0.46	0.35
Al <sub>2</sub> O <sub>3</sub>	13.56	13.11	1.17	9.33	2.60	5.20	1.27
Fe <sub>2</sub> O <sub>3</sub> tot	17.37	13.89	2.99	12.79	0.75	10.78	1.64
MnO	0.33	0.21	0.04	0.25	0.06	0.24	0.06
MgO	11.03	6.29	1.35	11.25	2.36	21.08	1.03
CaO	6.85	7.81	1.79	8.90	0.98	10.21	0.99
Na <sub>2</sub> O	1.04	3.02	1.07	2.22	1.33	0.33	0.14
K <sub>2</sub> O	0.19	0.97	0.78	0.21	0.12	0.06	0.03
P <sub>2</sub> O <sub>5</sub>	0.19	0.15	0.06	0.12	0.02	0.05	0.03
LOI	2.96	1.48	1.05	1.20	0.73	3.09	0.76
Elements ppm							
Ba	10	251	186	36	21	5	4
Rb	12	30	23	7	6	3	1
Sr	65	169	98	77	47	12	9
Ga	23	23	4	12	3	11	2
Nb	7	7	3	7	3	4	3
Zr	144	146	37	110	31	50	30
Cr	308	256	258	1078	643	2748	634
Ni	174	99	47	318	206	1199	307
Zn	305	152	61	152	45	123	22
Y	12	27	10	18	3	13	7
Th	4	6	2	6	4	7	9
La	12.5	19.4	6.9	17.1	8.7	4.8	3.7
Ce	28.0	38.8	13.4	38.5	18.4	12.6	9.8
Pr	3.4	4.9	1.6	4.7	2.0	1.4	1.0
Nd	14.8	19.5	6.6	18.1	6.4	6.0	3.7
Sm	3.4	4.8	1.4	4.2	1.0	1.7	0.9
Eu	1.2	1.5	0.5	1.3	0.3	0.5	0.3
Gd	3.6	5.1	1.4	4.0	0.7	2.0	0.9
Dy	2.9	4.8	1.4	3.3	0.4	2.0	0.9
Er	1.4	2.7	1.3	1.6	0.3	1.1	0.5
Yb	1.1	2.3	1.1	1.3	0.2	1.3	0.9
Lu	0.2	0.3	0.2	0.2	0.0	0.2	0.2

SD\* standard deviation; LOI loss on ignition; tot total content.

To place mineralogical data of the suspect pillow lava into a geochemical context, we briefly present and summarize data on komatiite, komatiitic basalts and tholeiites from [10]. The tholeiite–komatiite suite indicates a relatively wide compositional range with SiO<sub>2</sub> content of 45.06–59.2 wt.% and a Mg# [MgO/(MgO + FeO<sub>tot</sub>) × 100] ratio of 17–71. All rocks are classified dominantly as sub-alkali basalt and andesitic basalts based on [41] (Figure 9a). The “andesitic” nomenclature is not supported by the mineralogy and other geochemical parameters but only as an expression of higher silica abundance. Similar silica levels in basal volcanic rocks have also been reported by [8]. On the classification diagram after [42], rocks plot a gradual transition from komatiites, komatiitic basalts up to high-Mg and high-Fe tholeiite fields (Figure 9b), with tholeiitic affinity based on high FeO content. Rocks from the Aravalli sequence also reveal variable MgO content: 3.9–7.9 wt.% for tholeiites, 9.0–11.9 wt.% for komatiitic basalts and 19.6–22.4 wt.% for komatiites. The AR-6C sample from inner part of the pillow-like lava is characterized by a relatively high MgO 11.03 wt.% and plots on the border of the komatiitic basalts and high Mg-tholeiites (Figure 9b).

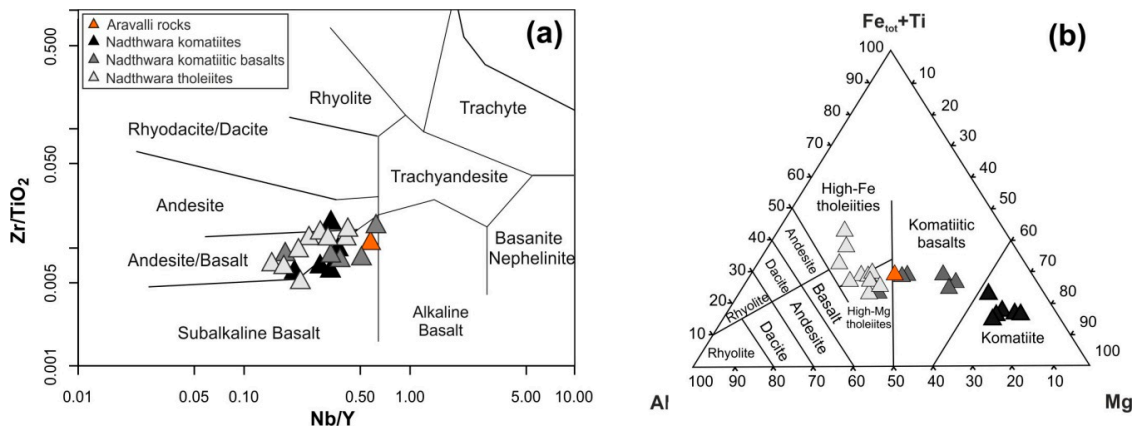


**Figure 9.** (a) Zr/TiO<sub>2</sub> vs Nb/Y plot after [41], (b) Al-(Fe<sub>tot</sub> + Ti)-Mg diagram after [42] for the AR-6C sample and Nathdwara volcanic rocks (data from [10]).

Most of the trace elements in a function of immobile Zr show a perfect linear trend (Figure 10). Only Rb does not show linear variation, which can be attributed to some degree of elemental mobility during metamorphism. A broad negative correlation between MgO and Zr suggests the role of the fractional crystallization process.

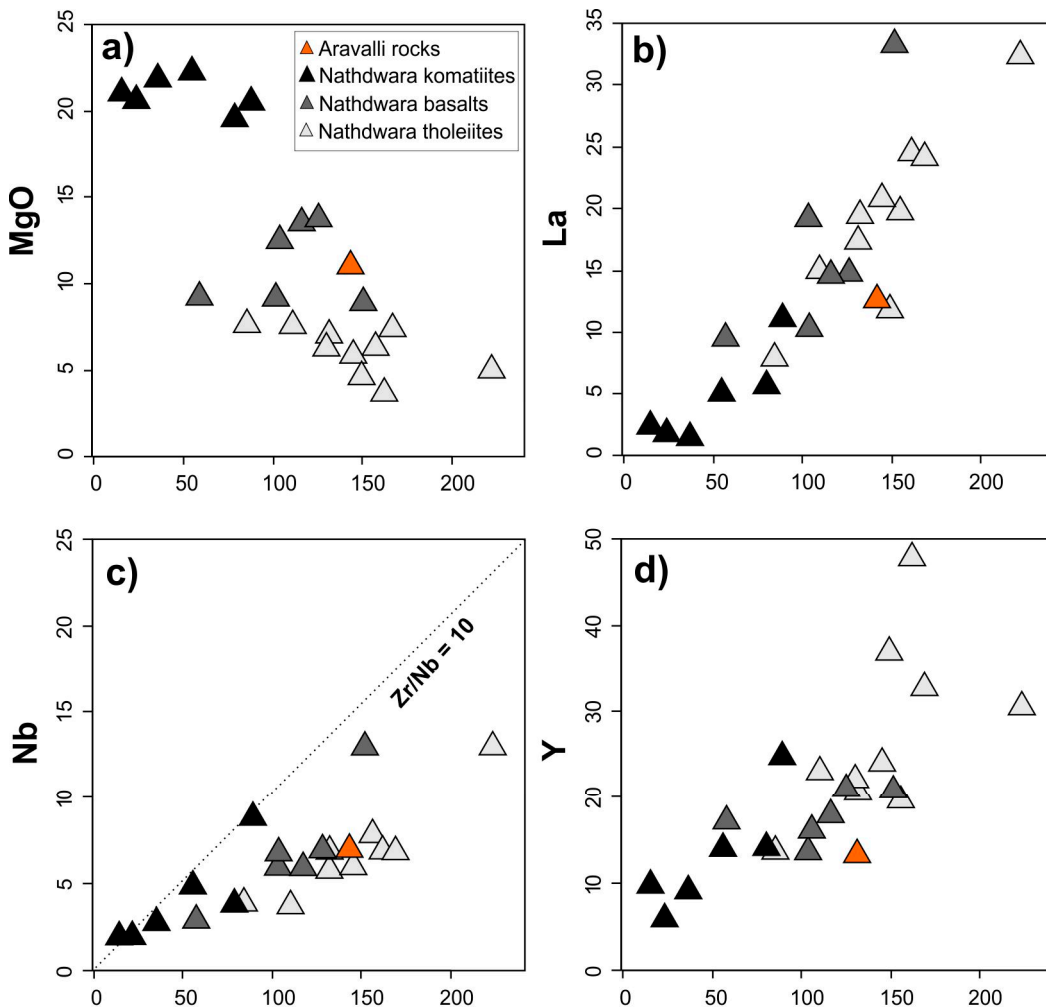


**Figure 10.** Cont.

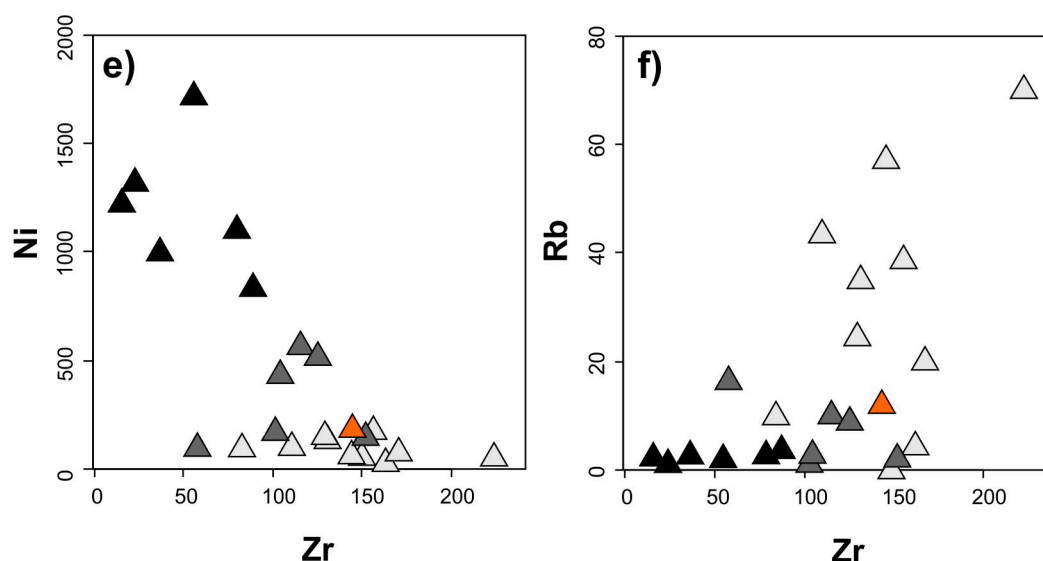


**Figure 10.** Bivariate plots of Zr (as an index of fractionation) versus selected elements for the AR-6C sample and Nathdwara rocks (data from [10]). (a) major oxide (MgO) vs. Zr, (b–f) trace elements (La, Nb, Y, Ni, Rb) vs. Zr.

All of the mafic volcanic rocks exhibit REE patterns with LREE enrichment (Figure 11 normalizing values from [43]), where tholeiites exhibit  $La/Sm_N = 1.54\text{--}2.85$  and  $La/Yb_N = 2.23\text{--}10.90$ , komatiitic basalts  $1.74\text{--}3.85$ ,  $5.78\text{--}14.91$  and komatiites  $1.11\text{--}2.37$ ,  $1.49\text{--}4.30$  respectively. The new Aravalli sample AR-6C indicates  $La/Sm_N = 2.3$  and  $La/Yb_N = 7.73$ , similar to the tholeiites and komatiitic basalts. In terms of the multi-element plots normalized against enriched mid-ocean ridge basalts (E-MORB) [44] (Figure 11), the Aravalli tholeiite and the komatiitic basalt samples plot parallel the E-MORB, i.e., along or above the normalized ratio line 1 for most of the incompatible trace elements, indicating their derivation from enriched mantle sources similar to those for the E-MORB (Figure 11), however, the Aravalli samples have prominent negative anomalies for Nb, P, Sr and to some extent Eu and Ti, commonly observed in continental rift volcanics [45].

However, the komatiitic samples plot mostly below the normalized ratio line 1, indicating their derivation from less enriched mantle sources by higher degrees of partial melting compared to the tholeiite and komatiitic basalt samples, although depicting similar depletion of Nb, Sr, Eu, P and Ti, like the tholeiite and komatiitic basalt, indicating rift tectonic environment [10]. The tectonic interpretation is confirmed by the Zr/Y vs. Zr plot [46] where the Aravalli samples plot within or close to the “Within-Plate Basalt” field (Figure 12).

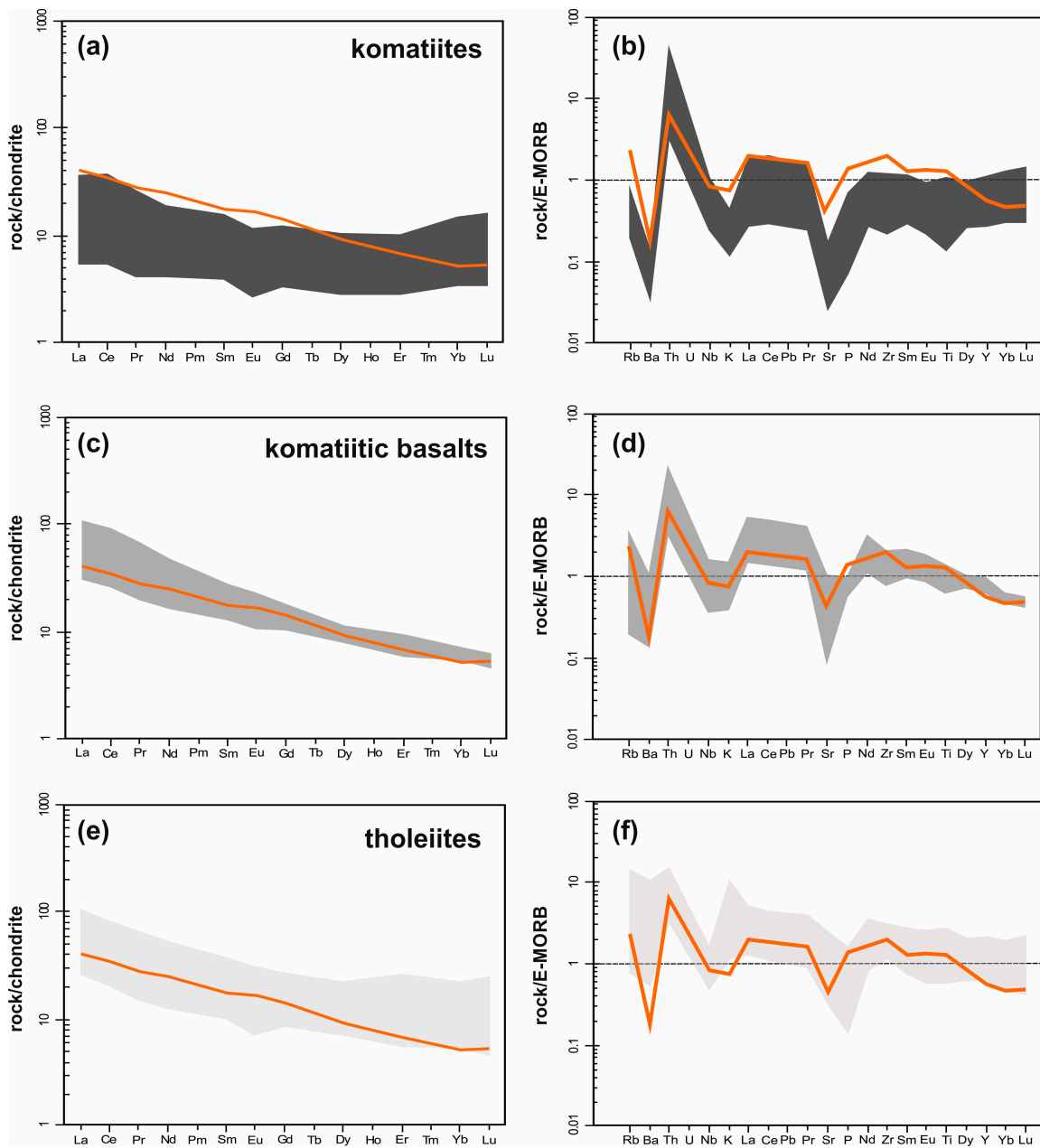


**Figure 11.** (a,c,e) chondrite-normalized REE patterns for komatiite, komatiitic basalts and tholeiite respectively (normalizing values after [43]), (b,d,f) E-MORB normalized multi-element spider diagrams (normalizing values after [44]) for the komatiite, komatiitic basalts and tholeiite respectively (data from [10]), REE and multi-element patterns of AR-6C (brown line) shown for comparison.

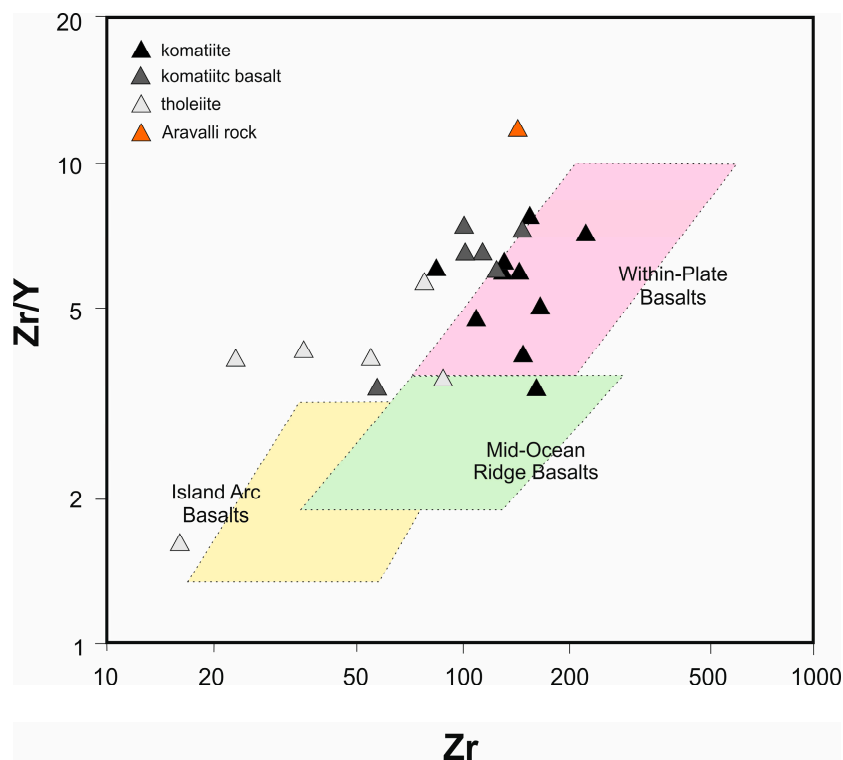


Figure 12. Zr/Y vs. Zr diagram after [46].

#### 4. Discussion

**Geotectonic settings:** The basal sequence of Aravalli is composed of mafic, ultramafic and komatiitic volcanites [8,10]. The geochemical criteria used in previous publications (i.e.,  $La/Nb = 1$  and  $Nb/Y = 0.3$  [47]) have suggested (in the case of komatiite) a simple connection of magmatism with the mantle plume and oceanic plateau basalt source. On the other hand, the komatiitic basalts and tholeiites resemble arc basalts with a typical  $La/Nb$  ratio of ca. 3. However, [16] based on lithological consideration, overall, the geology, petrology and geochemical arguments, including similar incompatible trace element ratios for continental rift basalt and arc basalt, link Aravalli volcanic rocks with rift-related magmatism. Furthermore, arc basalt indicates an overall relatively lower abundance of the incompatible trace elements compared to rift basalt, but arc basalt has similar multi-element patterns and arc basalts frequently contain positive Eu and Sr anomalies because of plagioclase accumulation, whereas these (Sr and Eu) have negative anomalies in rift basalt as in the case of Aravalli basalt [10]. Aravalli rocks, presented in this study, show general enrichment of LREE and LILE patterns and pronounced negative Nb, Sr, Eu, P and Ti anomalies, which are characteristic of many continental flood basalt suites, dyke swarms and rift volcanics [10,48–50].

**Mineralogy:** the mineralogy of the Aravalli rocks contributes towards understanding the geotectonic environment, whether the Aravalli meta-volcanic rocks are rift or subduction related. The subduction-related komatiite and their origin in shallower melting regimes is possible through the incorporation of significant amounts of  $H_2O$ . Most of the komatiites contain hydrous amphiboles, but they are products of metamorphism rather than indicators of the real high  $H_2O$  content of magma. Thus, the determination of the possible water content in the system can be possible only on the basis of primary minerals. In the case of Aravalli pillow lava, the only mineral that may indicate the crystallization environment is the clino-pyroxene relicts. The first experimental studies indicating the possible high  $H_2O$  content in komatiites come from Barberton komatiites [51,52], where augite with high Wo content ( $>0.4$ ) was found as the only pyroxene. The experiments, carried out after the addition of water, displayed a very good match with a natural augite composition. On the contrary, the anhydrous experiments produced two pyroxenes, both pigeonite and augite (with lower CaO

content of Wo = 0.3–0.35). Taking into account that the pyroxene relics found in Aravalli pillow lava had both augite and subordinate pigeonite and even enstatite compositions, and that the augite has a low Ca content (Wo about 0.3), it can be stated that their crystallization took place in an anhydrous environment, considered as associated to the mantle plume. Based on the chemical composition of amphiboles, which are the result of metamorphism, it can be stated that the rocks within this area were subjected to later temperatures not in excess of 550–600 °C and pressures in the range of 3.0–7.0 kbar for the majority of amphiboles and 8.0–10.7 kbar for the minority, typical of amphibolite facies metamorphism.

**Textural relationship:** distinctive spinifex-like texture on a weathered Aravalli pillow lava surface consists of long, platy or fibrous phenocrysts of amphibole, however, olivine spinifex-texture is usually typical of komatiite lavas from most greenstone Archean belts worldwide. In the case of Aravalli, the mineralogical composition of rocks with a spinifex type textures has been strongly perturbed through repetitive episodes of regional metamorphism over millions of years, as well as hydrothermal and weathering changes. Primary minerals such as pyroxene, of which relics were observed at places, are replaced by secondary minerals such as chlorite and Ca-amphibole and carbonates. These Aravalli rock features were, at first, thought to have a komatiitic affinity by their resemblance to other spinifex textured komatiitic occurrences in the world, i.e., [53–55], but their geochemical composition indicates komatiitic/tholeiitic affinity with MgO content ranges up to 22 wt.%, reported by [10] and a wide range of SiO<sub>2</sub> (45.06–59.2 wt.%). A few cases of spinifex-textured volcanic rocks are reported in the world literature, with significantly variable geochemical compositions compared to those of typical komatiites, e.g., in volcanic rocks with Ca-amphibole spinifex from the province of Musgraves in Western Australia [56] or platy pyroxene spinifex in the Boundle Volcanic Member of the Meekatharra Formation [57]. These rocks have moderate to high MgO content and show that spinifex texture occurs over a broad compositional spectrum. The formation of preferentially-oriented crystals typical of platy spinifex cannot be attributed exclusively to the nature or composition of the komatiite liquid. An explanation for its origin is related to specific physical conditions that prevailed during the crystallization of the upper part of the lava flow. The experiments [58] demonstrate that spinifex is a natural consequence of crystallization in the thermal gradient of a hot, dry and ultramafic lava flow. The large crystals are oriented perpendicular to the cooling front. The fibrous and skeletal post-pyroxene amphibole showed that this mineral was growing rapidly, under high degrees of undercooling [58]. To form pillows in true high Mg-rich komatiites, a lower local flow rate is required [59]. Such low flow rates are in conflict with the high flow velocities generally assumed for komatiites, and hence explains the rarity of submarine komatiite pillow lavas. In the case of Aravalli, a whole rock geochemistry documents tholeiites. Thus, these relatively small pillow forms may document a sub-marine or shallower lake-like eruption environment. The proposed model by [16], for the geotectonic evolution of the Aravalli belt, is consistent with the rifting model of [60], suggesting deep mantle plume melting of mantle material and the thinning of lithosphere, ultimately leading to continental rifting. Magmas may reach the surface as flood basalts.

**Supplementary Materials:** The following are available online at <http://www.mdpi.com/2075-163X/10/7/638/s1>. Table S1: Results of the EPMA analyses of Aravalli amphibole, Table S2: Results of the EPMA analyses of Aravalli pyroxene, Table S3: Results of the EPMA analyses of Aravalli feldspar, Table S4: Results of the EPMA analyses of Aravalli chlorite, Table S5: Results of the EPMA analyses of Aravalli ilmenite, Table S6: Results of the P-T condition estimations.

**Author Contributions:** Conceptualization, J.W., E.K., A.G. and T.A.; methodology, E.K., J.W., and A.G. software, A.G.; validation, J.W., and T.A., formal analysis, J.W., E.K., and A.G.; investigation, J.W., T.A., E.K., A.G., resources, T.A. and J.W.; data curation, J.W., T.A.; writing—original draft preparation, J.W., E.K., A.G., writing—A.G.; visualization, A.G., E.K.; supervision, J.W., and T.A. project administration, J.W.; funding acquisition, J.W.; All authors have read and agreed to the published version of the manuscript.

**Funding:** This work benefited from Indo-Polish Joint Research Project of Department of Science & Technology, New Delhi (No. INT/POL/P-14/05) to T.A. & J.W. This research was funded by the Ministry of Science and Higher Education (Poland) grant number 62.9012.2012.000 for J.W. in 2020.

**Acknowledgments:** The authors are thankful to Lidia Jeżak for her help in performing EPMA analyses at the Electron Microprobe Laboratory of the Inter-Institute Analytical Complex for Minerals and Synthetic Substances in University of Warsaw and Grzegorz Zielinski for qualitative and quantitative analysis of elemental composition using a WDS equipment with CAMECA SX 100 electron microprobe at Polish Geological Institute in Warsaw, Poland.

**Conflicts of Interest:** The authors declare no conflict of interest.

## References

1. De Wit, M.J.; Ashwal, L.D. Greenstone belts: What are they? *South. Afr. J. Geol.* **1995**, *98*, 505–520.
2. Kerrich, R.; Polat, A.; Wyman, D.; Hollings, P. Trace element systematics of Mg to Fe–tholeiitic basalt suites of the Superior Province: Implications for Archean mantle reservoirs and greenstone belt genesis. *Lithos* **1999**, *46*, 163–187. [[CrossRef](#)]
3. Polat, A. Growth of Archean continental crust in oceanic island arcs. *Geology* **2012**, *40*, 383–384. [[CrossRef](#)]
4. Condie, K.C. TTG and adakites: Are they both slab melts? *Lithos* **2005**, *80*, 33–44. [[CrossRef](#)]
5. Condie, K.C.; Kröner, A. The building blocks of continental crust: Evidence for a major change in the tectonic setting of continental growth at the end of the Archean. *Gondwana Res.* **2013**, *23*, 394–402. [[CrossRef](#)]
6. Tewari, H.C.; Prasad, B.R.; Kumar, P. *Structure and Tectonics of the Indian Continental Crust and Its Adjoining Region: Deep Seismic Studies*, 1st ed.; Elsevier: Amsterdam, The Netherlands, 2008; pp. 57–72.
7. Fareeduddin; Banerjee, D.M. Aravalli craton and its mobile belts: An update. *Episodes* **2020**, *43*, 88–108. [[CrossRef](#)]
8. Ahmad, T.; Rajamani, V. Geochemistry and petrogenesis of the basal Aravalli Volcanics near Nathdwara, Rajasthan, India. *Precambrian Res.* **1991**, *49*, 185–204. [[CrossRef](#)]
9. Malviya, V.P.; Arima, M.; Pati, J.K.; Kaneko, Y. Petrology and Geochemistry of metamorphosed basaltic pillow lava and basaltic komatiite in the Mauranipur area: Subduction related volcanism in the Archean Buldenkhand Craton, central India. *J. Miner. Petrol. Sci.* **2006**, *102*, 191–217. [[CrossRef](#)]
10. Ahmad, T.; Tarney, J. Geochemistry and petrogenesis of Late Archaean Aravalli Volcanics, basement enclaves and granitoids, Rajasthan. *Precambrian Res.* **1994**, *65*, 1–23. [[CrossRef](#)]
11. Gopalan, K.; Macdaugall, J.D.; Roy, A.B.; Murali, A.V. Sm-Nd evidence for 3.3 Ga old rock in Rajasthan, north-western India. *Precambrian Res.* **1990**, *48*, 287–297. [[CrossRef](#)]
12. Wiedenbeck, M.; Goswami, J.N. An ion-probe single zircon  $^{207}\text{Pb}/^{206}\text{Pb}$  age from Mewar Gneiss at Jhamarkotra, Rajasthan. *Geochim. Cosmochim. Acta* **1994**, *58*, 2135–2141. [[CrossRef](#)]
13. Roy, A.B.; Kröner, A. Single zircon evaporation ages constraining the growth of the Archaean Aravalli craton, northwestern Indian shield. *Geol. Mag.* **1996**, *133*, 333–342. [[CrossRef](#)]
14. Roy, A.B.; Kröner, A.; Laul, V. Detrital zircons constraining basement age in a late Archaean greenstone belt of south-eastern Rajasthan, India. *Curr. Sci.* **2001**, *81*, 407–410.
15. Heron, A.M. Geology of Central Rajputana. *Geol. Surv. India. Mem.* **1953**, *79*, 389.
16. Ahmad, T.; Dragusanu, C.; Tanaka, T. Provenance of Proterozoic Basal Aravalli mafic volcanic rocks from Rajasthan, Northwestern India: Nd isotopes evidence for enriched mantle reservoirs. *Precambrian Res.* **2008**, *162*, 150–159. [[CrossRef](#)]
17. Ahmad, T.; Deb, M.; Tarney, J.; Raza, M. Proterozoic mafic volcanism in the Aravalli-Delhi Orogen, north-western India: Geochemistry and tectonic framework. *J. Geol. Soc. India* **2008**, *72*, 93–111.
18. Deb, M.; Sarkar, S.C. Proterozoic tectonic evolution and metallogenesis in the Aravalli–Delhi orogenic Complex, Northwestern India. *Precambrian Res.* **1990**, *46*, 115–137. [[CrossRef](#)]
19. Naha, K.; Halyburton, R.V. Early Precambrian stratigraphy of central and southern Rajasthan. *Precambrian Res.* **1974**, *1*, 55–73. [[CrossRef](#)]
20. Sugden, T.J.; Deb, M.; Windley, B.F. The tectonic setting of mineralisation in the Proterozoic Aravalli Delhi Orogenic belt, NW India. In *Developments in Precambrian Geology*; Elsevier: Amsterdam, The Netherlands, 1990; Volume 8, pp. 367–390. [[CrossRef](#)]
21. Shore, M.; Fowler, A.D. The origin of spinifex texture in komatiites. *Nature* **1999**, *397*, 691–694. [[CrossRef](#)]
22. Bouquain, S.; Arndt, N.T.; Faure, F.; Libourel, G. An experimental study of pyroxene crystallization during rapid cooling in a thermal gradient: Application to komatiites. *J. Geophys. Res. Solid Earth* **2014**, *5*, 641–650. [[CrossRef](#)]

23. Hawthorne, F.C.; Oberti, R.; Harlow, G.E.; Maresch, W.V.; Martin, R.F.; Schumacher, J.C.; Welch, M.D. Nomenclature of the amphibole supergroup. *Am. Mineral.* **2012**, *97*, 2031–2048. [CrossRef]
24. Morimoto, N. Nomenclature of pyroxenes. *Mineral. J.* **1989**, *14*, 198–221. [CrossRef]
25. Hey, M.H. A new review of the chlorites. *Mineral. Mag.* **1954**, *30*, 277–292. [CrossRef]
26. Tindle, A.G. Mineral Recalculation Software of Chlorite (Chlorite.xls). Available online: <http://www.open.ac.uk/earth-research/tindle/AGTWebPages/AGTSoft.html> (accessed on 30 March 2020).
27. Cassidy, K.F.; Groves, D.I.; Binns, R.A. Manganian ilmenite formed during regional metamorphism of Archean mafic and ultramafic rocks from Western Australia. *Can. Mineral.* **1988**, *26*, 999–1012.
28. Blundy, J.D.; Holland, T.J. Calcic amphibole equilibria and a new amphibole-plagioclase geothermometer. *Contrib. Mineral. Petr.* **1990**, *104*, 208–224. [CrossRef]
29. Otten, M.T. The origin of brown hornblende in the Artfjället gabbro and dolerites. *Contrib. Mineral. Petr.* **1984**, *86*, 189–199. [CrossRef]
30. Hammarstrom, J.M.; Zen, E.A. Aluminum in hornblende: An empirical igneous geobarometer. *Am. Mineral.* **1986**, *71*, 1297–1313.
31. Hollister, L.S.; Grissom, G.C.; Peters, E.K.; Stowell, H.H.; Sisson, V.B. Confirmation of the empirical correlation of Al in hornblende with pressure of solidification of calc-alkaline plutons. *Am. Mineral.* **1987**, *72*, 231–239.
32. Mutch, E.J.F.; Blundy, J.D.; Tattich, B.C.; Cooper, F.J.; Brooker, R.A. An experimental study of amphibole stability in low-pressure granitic magmas and a revised Al-in-hornblende geobarometer. *Contrib. Mineral. Petr.* **2016**, *171*, 85. [CrossRef]
33. Krawczynski, M.J.; Grove, T.L.; Behrens, H. Amphibole stability in primitive arc magmas: Effects of temperature, H<sub>2</sub>O content, and oxygen fugacity. *Contrib. Mineral. Petrol.* **2012**, *164*, 317–339. [CrossRef]
34. Chivas, A.R. Geochemical evidence for magmatic fluids in porphyry copper mineralization. *Contrib. Mineral. Petrol.* **1982**, *78*, 389–403. [CrossRef]
35. Wang, Z.M.; Han, C.M.; Xiao, W.J.; Su, B.X.; Ding, J.X.; Song, S.H. Geochemical and zircon U-Pb and Lu-Hf isotopic constraints on the origin of supracrustal rocks from the mid-Qilian terrane: A comparison between supracrustal rocks on the two sides of the eastern segment of the Altyn Tagh Fault. *Precambrian Res.* **2017**, *294*, 284–306. [CrossRef]
36. Xue, Z.J.; Bai, R.X.; Chen, W. *Genetic Mineralogy*, 1st ed.; University of Geosciences Press: Beijing, China, 1990; pp. 1–161. (In Chinese)
37. Chen, G.Y.; Sun, D.S.; Yin, H.A. *Genetic Mineralogy and Prospecting Mineralogy*, 1st ed.; University of Chongqing Publishing House: Chongqing, China, 1987; pp. 1–872. (In Chinese)
38. Zang, W.; Fyfe, W.S. Chloritization of the hydrothermally altered bedrock at the Igarape Bahia gold deposit, Carajas, Brasil. *Miner. Deposita* **1995**, *30*, 30–38. [CrossRef]
39. Kranidiotis, P.; MacLean, W.H. Systematics of chlorite alteration at the Phelps Dodge massive sulfide deposit, Matagami, Quebec. *Econ. Geol.* **1987**, *82*, 1898–1911. [CrossRef]
40. Cathelineau, M.; Nieva, D. A chlorite solid solution geothermometer. *Contrib. Mineral. Petr.* **1985**, *91*, 235–244. [CrossRef]
41. Winchester, J.A.; Floyd, P.A. Geochemical discrimination of different magma series and their differentiation products using immobile elements. *Chem. Geol.* **1977**, *20*, 325–343. [CrossRef]
42. Jensen, L.S. A new cation plot for classifying subalkalic volcanic rocks. In *Ontario Division Mines, Miscellaneous Paper*; Ministry of Natural Resources: Toronto, Canada, 1976; pp. 1–21.
43. Boynton, W.V. Cosmochemistry of the rare earth elements: Meteorite studies. In *Rare Earth Element Geochemistry*, 1st ed.; Henderson, P., Ed.; Elsevier: Amsterdam, The Netherlands, 1984; pp. 63–114.
44. Sun, S.S.; McDonough, W.F. Chemical and isotopic systematics of oceanic basalts: Implications for mantle composition and processes. *Geol. Soc. Spec. Publ.* **1989**, *42*, 313–345. [CrossRef]
45. Ahmad, T.; Tarney, J. Geochemistry and petrogenesis of Garhwal volcanics: Implications for evolution of the north Indian lithosphere. *Precambrian Res.* **1991**, *50*, 69–88. [CrossRef]
46. Pearce, J.A.; Norry, M.J. Petrogenetic implications of Ti, Zr, Y, and Nb variations in volcanic rocks. *Contrib. Mineral. Petr.* **1979**, *69*, 33–47. [CrossRef]
47. Condie, K.C. Mafic crustal xenoliths and the origin of the lower continental crust. *Lithos* **1999**, *46*, 95–101. [CrossRef]

48. Thompson, R.N.; Morrison, M.A.; Dickin, A.P.; Hendry, G.L. Continental flood basalt . . . Arachnids rule OK? In *Continental Basalts and Mantle Xenoliths*, 1st ed.; Hawkesworth, C.J., Morry, M.J., Eds.; Shiva: Nantwich, UK, 1983; pp. 158–185.
49. Weaver, B.L.; Tarney, J. Chemistry of the sub-continental mantle: Inferences from Archean and Proterozoic dykes and continental flood basalts. In *Continental Basalts and Mantle Xenoliths*, 1st ed.; Hawkesworth, C.J., Morry, M.J., Eds.; Shiva: Nantwich, UK, 1983; pp. 209–229.
50. Dupuy, C.; Dostal, J. Trace element geochemistry of some continental tholeiites. *Earth Planet. Sci. Lett.* **1984**, *67*, 61–69. [[CrossRef](#)]
51. Parman, S.W.; Dann, J.C.; Grove, T.L.; De Wit, M.J. Emplacement conditions of komatiite magmas from the 3.49 Ga Komati Formation, Barberton Greenstone Belt, South Africa. *Earth Planet. Sci. Lett.* **1997**, *150*, 303–323. [[CrossRef](#)]
52. Parman, S.W.; Grove, T.L. Komatiites in the plume debate. *Geol. Soc. Am. Spec. Pap.* **2005**, *388*, 249–256.
53. Viljonen, M.J.; Viljonen, R.P. The geology and geochemistry of the lower ultramafic unit of the Onverwacht group and proposed new class of igneous rocks. *Spec. Publ. Geol. Soc. S. Afr.* **1969**, *2*, 55–85.
54. Arndt, N.T.; Nisbet, E.G. Komatiites. What is 350 a komatiite. In *Komatiites*, 1st ed.; Arndt, N.T., Nisbet, E.G., Eds.; George Allen & Unwin: London, UK, 1982; pp. 19–28.
55. Arndt, N.T.; Leshner, C.M.; Barnes, S.J. *Komatiite*, 1st ed.; Cambridge University Press: Cambridge, UK, 2008; pp. 1–196.
56. Howard, H.M.; Werner, M.; Smithies, R.H.; Evins, P.M.; Kirkland, C.L.; Kelsey, D.E.; Hand, M.; Collins, A.; Pirajno, F.; Wingate, M.T.D.; et al. *The Geology of the West Musgrave Province and the Bentley Supergroup—A Field Guide*; Geological Survey of Western Australia: Adelaide, Australia, 2011; pp. 1–125.
57. Lowrey, J.R.; Ivanic, T.J.; Wyman, D.A.; Roberts, M.P. Platy pyroxene: New insights into Spinifex texture. *J. Petrol.* **2017**, *58*, 1671–1700. [[CrossRef](#)]
58. Faure, F.; Arndt, N.; Libourel, G. Formation of spinifex texture in komatiites: An experimental study. *J. Petrol.* **2006**, *47*, 1591–1610. [[CrossRef](#)]
59. Staude, S.; Jones, T.J.; Markl, G. The textures, formation and dynamics of rare high-MgO komatiite pillow lavas. *Precambrian Res.* **2020**, *343*. [[CrossRef](#)]
60. White, R.; McKenzie, D. Magmatism at rift zones: The generation of volcanic continental margins and flood basalts. *J. Geoph. Res.* **1989**, *94*, 7685–7729. [[CrossRef](#)]



© 2020 by the authors. Licensee MDPI, Basel, Switzerland. This article is an open access article distributed under the terms and conditions of the Creative Commons Attribution (CC BY) license (<http://creativecommons.org/licenses/by/4.0/>).